Eddy Transport and Mixing in a Wind- and Buoyancy-Driven Jet on the Sphere

IVANA CEROVEČKI,* R. ALAN PLUMB, AND WILLIAM HERES

Program in Atmospheres, Oceans, and Climate, Department of Earth, Atmospheric, and Planetary Sciences, Massachusetts Institute of Technology, Cambridge, Massachusetts

(Manuscript received 10 April 2006, in final form 1 October 2008)

ABSTRACT

The baroclinically unstable wind- and buoyancy-driven flow in a zonally reentrant pie-shaped sector on a sphere is numerically modeled and then analyzed using the transformed Eulerian-mean (TEM) formalism. Mean fields are obtained by zonal and time averaging performed at fixed height. The very large latitudinal extent of the basin (50.7°S latitude to the equator) allows the latitude variation of the Coriolis parameter to strongly influence the flow. Persistent zonal jets are observed in the statistically steady state. Reynolds stress terms play an important role in redistributing zonal angular momentum: convergence of the lateral momentum flux gives rise to a strong eastward jet, with an adjacent westward jet equatorward and weaker multiple jets poleward. An equally prominent feature of the flow is a strong and persistent eddy that has the structure of a Kelvin cat's eye and generally occupies the zonal width of the basin at latitudes 15°–10°S.

A strongly mixed surface diabatic zone overlies the near-adiabatic interior, within which Ertel potential vorticity (but not thickness) is homogenized along the mean isopycnals everywhere in the basin where eddies have developed (and thus is not homogenized equatorward of the most energetic eastward jet). A region of low potential vorticity (PV) is formed adjacent to the strong baroclinic front associated with that jet and subsequently maintained by strong convective events.

The eddy buoyancy flux is dominated by its skew component over large parts of the near-adiabatic interior, with cross-isopycnal components present only in the vicinity of the main jet and in the surface diabatic layer. Close to the main jet, the cross-isopycnal components are dominantly balanced by the triple correlation terms in the buoyancy variance budget, while the advection of buoyancy variance by the mean flow is not a dominant term in the eddy buoyancy variance budget.

Along-isopycnal mixing in the near-adiabatic interior is estimated by applying the effective diffusivity diagnostic of Nakamura. The effective diffusivity is large at the flanks of the mean jet and beneath it and small in the jet core. The apparent horizontal diffusivity for buoyancy obtained from the flux–gradient relationship is the same magnitude as the effective diffusivity, but the structures are rather different. The diapycnal diffusivity is strongest in the surface layer and also in a convectively unstable region that extends to depths of hundreds of meters beneath the equatorward flank of the main jet.

1. Introduction

Large-scale models used to study the circulation of the ocean must parameterize the effects of unresolved baroclinic eddies that effect the time-mean circulation through the transfer of heat and dynamic tracers, such as potential vorticity (PV). Much progress has been made recently in understanding the role of mesoscale eddies in developing and maintaining the ocean stratification (e.g., Karsten et al. 2002; Marshall and Radko 2003; Radko and Marshall 2004; Kuo et al. 2005; Eden et al. 2007b) as well as in developing the theory and parameterization of eddy transport (e.g., Gent and McWilliams 1990; Gent et al. 1995; McDougall and McIntosh 1996; Treguier et al. 1997; Visbeck et al. 1997; Greatbatch 1998; Wilson and Williams 2004; Plumb and Ferrari 2005; Eden et al. 2007a).

With the aim of developing further our understanding of eddy transport and its impact on the mean state of the ocean, we here build on two recent studies. Plumb and Ferrari (2005) have developed a nongeostrophic

* Current affiliation: Climate, Atmospheric Science and Physical Oceanography, Scripps Institution of Oceanography, University of California, San Diego, La Jolla, California.

Corresponding author address: Ivana Cerovečki, CASPO, Scripps Institution of Oceanography, UCSD, 9500 Gilman Drive, La Jolla, CA 92093.
E-mail: icerovec@ucsd.edu

DOI: 10.1175/2008JPO3596.1

transformed Eulerian-mean (TEM) theory for analysis of eddy transport of zonal mean flow, while Kuo et al. (2005) applied the theory to diagnose the equilibrium state of a wind- and buoyancy-driven, baroclinically unstable reentrant flow on an f plane. Like Treguier et al. (1997), Kuo et al. found that the role of eddies in that case could be interpreted in a straightforward way in terms of mixing of PV in the near-adiabatic interior and mixing of buoyancy in a diabatic surface layer.

In the present study, we consider a baroclinically unstable flow on the sphere. The model setup is briefly described in section 2; the modeled ocean is a sector of the sphere lying between the equator and 50.7°S and having 10° width in longitude (with longitudinally periodic boundary conditions). The flow, forced by a zonally homogeneous eastward wind stress and thermal relaxation to a zonally homogeneous temperature field specified at the surface, becomes baroclinically unstable and eventually reaches a statistically steady state characterized by oceanically realistic flow speeds and stratification; these and other aspects of the equilibrium state are described in section 3.

One important feature of the equilibrated flow is that over much of the domain the mean Ertel potential vorticity is homogenized along the mean isopycnals. Eddy heat fluxes are predominantly skew in the near-adiabatic interior with a significant diapycnal component only in the surface layer (section 3). The role of eddies in maintaining the equilibrium state is discussed in section 4 within the framework of the TEM formalism. The residual circulation and residual fluxes of buoyancy and PV are weak in the near-adiabatic interior except in the vicinity of the main jet. ''Eddy drag,'' which represents eddy forcing in the momentum equation and can be represented as a function of residual PV flux along the mean isopycnals and the diapycnal buoyancy flux (Plumb and Ferrari 2005), is weak except near the top and bottom boundaries.

To quantify the along-isopycnal, eddy-induced mixing in the flow, we estimate the effective diffusivity diagnostic developed by Nakamura (1996) and Winters and D'Asaro (1996). This is done by introducing a tracer into the flow, conserved everywhere but in the top model layer, except for a weak diffusivity, and using the resulting tracer structure to determine the spatially dependent effective diffusivity, as described in section 5. In agreement with chaotic advection theory, with experience in atmospheric applications (Haynes and Shuckburgh 2000a,b) and with the recent results of Marshall et al. (2006) for the Antarctic Circumpolar Current, effective diffusivity is found to be large on the flanks of, and beneath, the main zonal jet with lower values in the core of the jet. We briefly compare the effective diffusivity estimates with the different lateral eddy diffusivity of heat obtained from the flux-gradient relationship (section 5d).

Diapycnal eddy diffusivity, diagnosed following Medvedev and Greatbatch (2004), as described in section 5e, is appreciable only in the surface diabatic layer and the adjacent region close to the surface characterized by vigorous and persistent convection. Our conclusions are summarized in section 6.

The present work builds on work by Kuo et al. (2005); therefore many aspects of the present study resemble the study of Kuo et al. (2005): There is a similarity in the model setup, in the dynamics of the equilibrated solution, and analysis of the flow using the TEM approach. One novel aspect of the present study is inclusion of the latitudinal variation of the Coriolis parameter, which makes it possible to discriminate between thickness and PV homogenization. Another is in applying the effective diffusivity construct of, for example, Nakamura (1996) to estimate eddy transport and along-isopycnal mixing in the flow and to attempt to relate these to the mean flow characteristics. We additionally diagnose the eddy buoyancy variance budget, noting the importance of triple correlation terms.

2. Model setup

The model used is the Massachusetts Institute of Technology general circulation model (MITgcm) (Marshall et al. 1997a,b) configured in spherical coordinates. We consider hydrostatic flow in a domain between 50.7°S and the equator on the sphere. The equation of state is linear: $\rho = \rho_0(1 - \alpha_T T)$, where ρ is density, ρ_0 is reference density, α_T is the thermal expansion coefficient, and T is temperature. Much of the discussion is in terms of the buoyancy b, linearly related to the temperature T by $b = g\alpha_T T$ in which g is the vertical acceleration of gravity. The boundary conditions on the velocity field are no slip at $-50.7°$ and free slip at the equator. The horizontal resolution of $^1/_6°$ is eddy permitting, but in the interests of computational economy we restrict the basin width to 10° of longitude with periodic boundary conditions. The modeled ocean has 15 vertical levels of variable depth between the surface and the flat ocean bottom at 4-km depth, where momentum is removed by a quadratic bottom drag with the drag coefficient $C_D = 0.01$.

Small-scale variance is dissipated by (in the vertical) harmonic and (in the horizontal) biharmonic diffusion of momentum and buoyancy as well as convective adjustment of unstably stratified regions of fluid columns. In the uppermost three layers, of 100-m total thickness, the vertical viscosity and diffusivity are taken to be

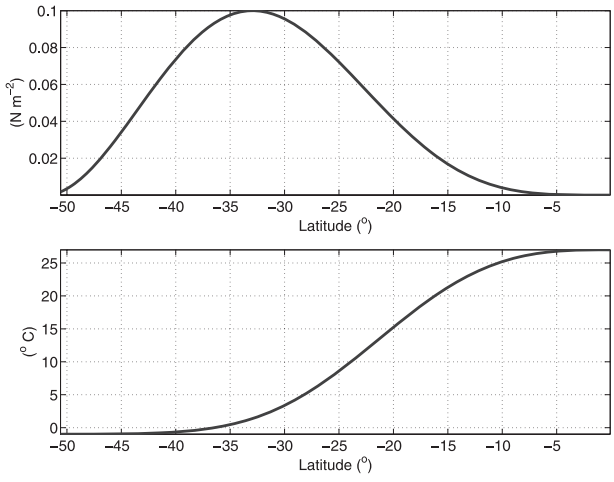

FIG. 1. The wind stress forcing τ_0 (N m^{-2}) and the restoring temperature (°C).

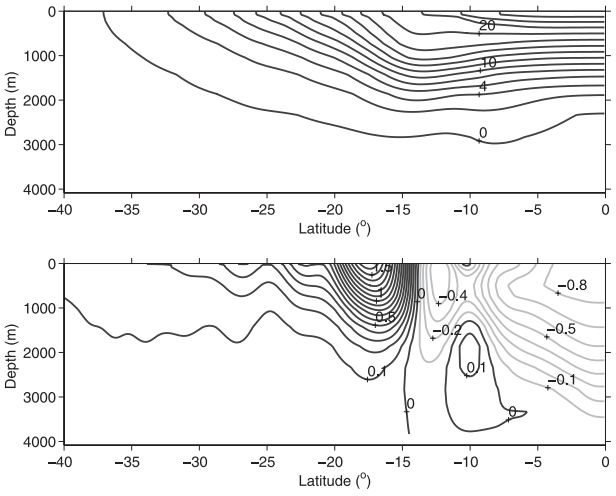

FIG. 2. Meridional cross section of (top) zonally and time-averaged temperature (contour interval 1°C) and (bottom) zonal velocity (contour interval 0.1 m s^{-1}). Negative velocities are plotted as light lines. Time averages were taken over 100 yr (years 1284–1384 of run).

$A_z = K_z = 10^{-2}$ m^2 s^{-1} in order to simulate a mixed layer. Elsewhere, $K_z = 3 \times 10^{-5}$ m^2 s^{-1} and $A_z = 10^{-3}$ m^2 s^{-1}. The biharmonic diffusion coefficients are $K_H = 10^{10}$ m^4 s^{-1} for temperature and $A_H = 2 \times 10^{11}$ m^4 s^{-1} for momentum.

The flow is forced at the surface by wind stress and buoyancy forcing. The buoyancy forcing is imposed by requiring the upper surface temperature to relax to a specified equilibrium distribution with the relaxation time of 30 days. The applied wind stress and equilibrium temperature are shown in Fig. 1. The wind stress is everywhere eastward (there is no westward stress in low latitudes) and becomes very small within about 10° of the equator; it reaches a maximum at 33°S, resulting in Ekman downwelling equatorward of the maximum and Ekman upwelling poleward.

The model was integrated from a state of rest and horizontally uniform stratification with realistic buoyancy frequency. The flow quickly became baroclinically unstable and the imposed forcing, in collusion with baroclinic eddies, resulted in a statistically steady state after several hundred years. All results presented here are taken after this steady state has been attained; the flow was integrated for 1285 years and the results were averaged in time over the last 100 years. Unless otherwise stated, the average denoted by an overbar is an average over both longitude and the last 100 years of the integration.

3. The equilibrium state description

a. Mean temperature and mean zonal velocity

The upper panel of Fig. 2 shows the equilibrium distribution of the mean temperature field. All ''mean'' fields are obtained by zonal and time averaging at fixed height. Convective adjustment in the cold southern part of the basin mixes the entire fluid column vertically to nearly uniform density. Between about 10° and 15°S latitude, the isotherms spread apart at depths from about 200 to 800 m, forming a well-defined pool of large thickness and, thus, of low PV. Closer to the equator both the wind and the surface heating are weak, and the fluid column remains uniformly stratified to great depth.

The lower panel of Fig. 2 shows the zonally and time-averaged zonal flow. A strong, deep, eastward jet is present just poleward of about 15°S with several additional eastward, albeit successively weaker, jets poleward of about 26°S. The mean zonal flow reverses direction suddenly on the equatorward side of the main jet where the flow is westward, giving rise to a westward jet near 13°S as well as in deep and extensive region of westward flow near the equator. Lateral eddy momentum flux takes positive zonal momentum out of equatorward region in the upper part of the water column. Although the mean meridional temperature gradient is very weak close to the equator, on account of small f the mean zonal flow may be nonzero in the region near the equator even at greater depths.

It is well known that both barotropic and baroclinic flows, whose forcing, as in this case, extends over many deformation radii in latitude, develop multiple jets (e.g., Panetta 1993), a result of the important role of Reynolds stresses in redistributing zonal angular momentum and thus determining the structure of the zonal mean flow. Zonally and time-averaged vertical sections of Reynolds

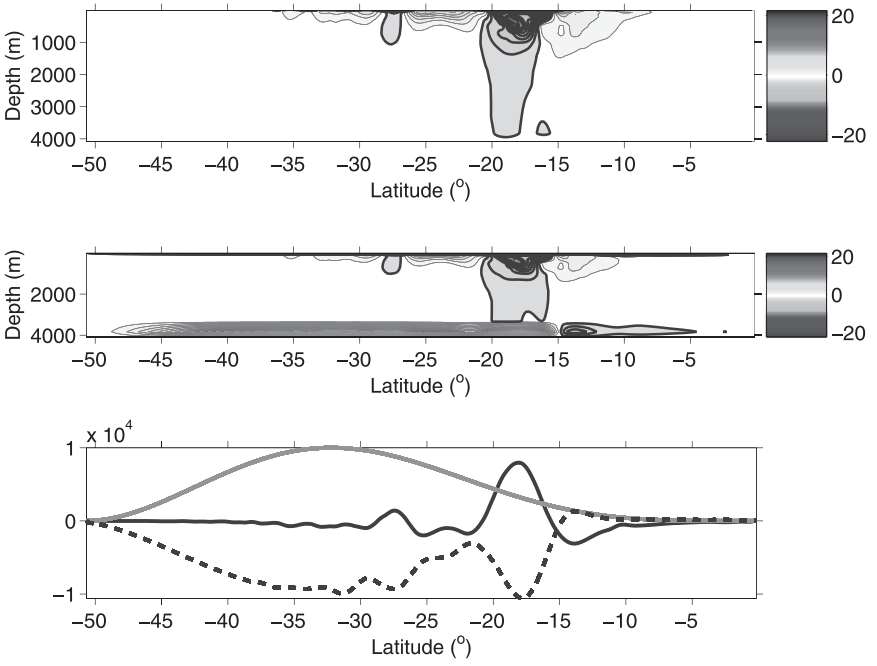

FIG. 3. Zonally and time-averaged vertical sections of (top) Reynolds stress divergence $\partial(\overline{u'v'})/\partial y + \partial(\overline{u'w'})/\partial z$ and (middle) Coriolis acceleration $f\bar{v}$, which are the terms that dominate the balance in the zonal momentum equation. Contour interval is 1 m s^{-2}; positive contours are shown as light lines and negative contours are shown as dark lines. All terms are multiplied by 10^8. (bottom) Dominant terms in the zonally and time-averaged vertically integrated zonal momentum balance, Eq. (1): the surface wind stress term: τ_0/ρ (light line), the vertically integrated Reynolds stress divergence term: $-(\partial/\partial_y)\int_{-D}^{0}\overline{u'v'}dz$ (dark solid line), and bottom drag term: $-\tau_{-D}/\rho$ (dashed line). All terms are multiplied by 10^8. (The vertically integrated Coriolis term must vanish by mass conservation.)

stress divergence $\partial(\overline{u'v'})/\partial y + \partial(\overline{u'w'})/\partial z$ (Fig. 3, top panel) and Coriolis acceleration $f\bar{v}$ (middle panel), show that these two terms are in very close balance everywhere in the flow except close to the surface (where vertical diffusion and wind stress play an important role) and close to the bottom (where bottom drag is important). The time averages of the three terms in the vertically integrated momentum balance,

$$-\frac{\partial}{\partial y}\int_{-D}^{0}\overline{u'v'}\,dz + \frac{1}{\rho}(\tau_0 - \tau_{-D}) = 0, \qquad (1)$$

where τ_0 is the applied wind stress and τ_{-D} the bottom stress, are shown in Fig. 3, bottom panel.

While the bottom stress mirrors the wind stress in its broad features, it also shows the presence of the jets (which extend down to the bottom, albeit weakly). The difference between top and bottom stress is balanced by the Reynolds stress divergence in the Eulerian-mean approach, as (1) implies. Angular momentum put in by the wind stress at the surface is thus redistributed latitudinally by the eddies and taken up by the bottom drag.

While the zonal mean flow has essentially equilibrated by this time, it is not in fact steady, but fluctuates quasiperiodically. The main eastward jet oscillates laterally about its mean position in a manner similar to what is found in simple models of the atmosphere, where fluctuations of the jet take the form of ''annular modes'' (e.g., Kushner and Polvani 2004) and which, in turn, appear to be analogs of similar behavior in the real atmosphere (e.g., Thompson and Wallace 2000). In our case, with multiple jets, the behavior is more complex: during each period, the secondary jets in fact migrate systematically equatorward, the northernmost one merging with the main jet while a new jet appears to the south. This behavior, a consequence of the mutual interaction between eddies and the jets, is explored further in Chan et al. (2007).

b. Eddy structures

Figure 4 shows a snapshot of sea surface temperature as a function of latitude and longitude (note that three zonal periods are plotted in the figure). Eddy activity is mostly confined between $-10°$ and $-35°$ latitude. The

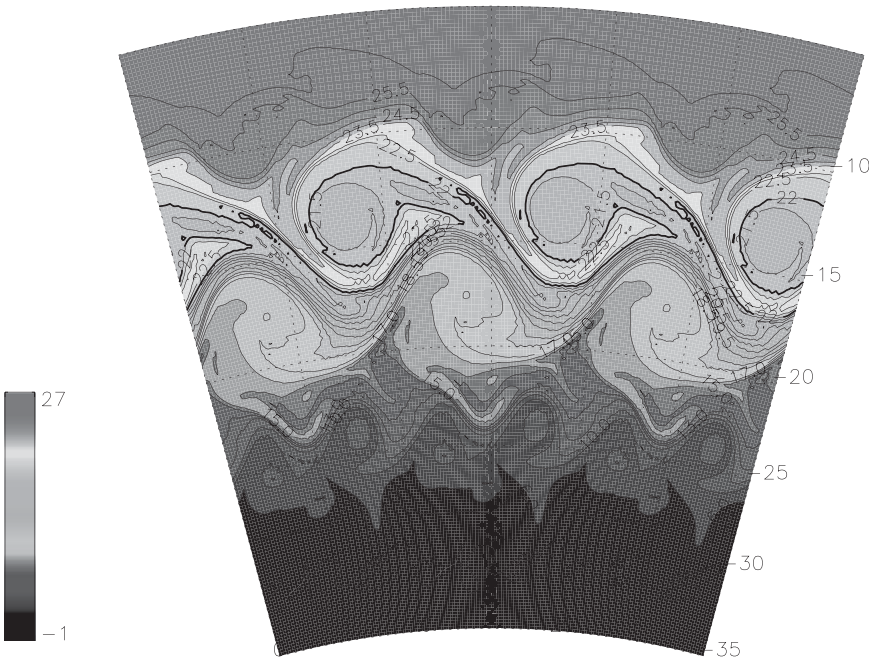

FIG. 4. A snapshot of sea surface temperature (°C): the periodic field is plotted 3 times in longitude, and only latitudes between −5° and −35°S are shown.

dominant and strongly persistent feature is a single cold eddy (i.e., zonal wavenumber 1 within the 10° longitude domain) found just equatorward of the main eastward jet. It is likely that the size of this eddy is determined by the geometry of the basin—at the beginning of the calculation it grew in size until it became zonally as large as the geometry permits. Poleward of the main jet, smaller-scale eddies are evident.

The circulation around the dominant cold eddy is anticyclonic. The temperature structure equatorward of the jet is very similar to that of a classic critical layer (Haynes 1985), the cold eddy taking the form of a Kelvin cat's eye—a lens-shaped region of closed streamlines enclosing a well-mixed region. In this critical layer between the eastward and westward jets where the mean flow is weak (the zonal phase speed of this eddy $c \simeq 0.1$ m s^{-1} eastward, and the critical layer forms where $\bar{u} \simeq c$), the flow is essentially trapped within the eddy. As Fig. 4 shows, both warm and cold water filaments are formed at the apex of the eddy (similar to the hyperbolic point in a steady flow). At the time of Fig. 4, the eddy is very close to the jet but it subsequently drifts slowly equatorward, weakens, and is advected eastward by the local flow. Subsequently, it reforms near the jet and the cycle repeats itself.

As the warm water filaments are wrapped around the eddy on its poleward side, they fill a growing region between the eddy and the eastward jet with warm water. This region, therefore, becomes prone to convection since the atmosphere above is colder than the surface water. Convective events and the subsequent sliding of water along isopycnals carry surface water downward into the interior, feeding the low PV pool that is visible as the weakly stratified region between latitudes 10°–15°S and depths 200–800 m in Fig. 2. This process is discussed further by Cerovečki and Marshall (2008).

c. *Eddy heat fluxes*

The zonal and time-averaged eddy temperature flux $\overline{\mathbf{u}'T'}$ is shown in Fig. 5 superposed on zonally and time-averaged isotherms (which coincide with the isopycnals in this calculation). The eddy heat flux (parallel to the eddy temperature flux) has a large, downgradient diapycnal component in the surface diabatic layer; however, it is ''skew'' (along the mean isopycnals) almost everywhere in the near-adiabatic interior, the exception being at the equatorward edge of the main jet at about 15°S, where the flux is cross isopycnal and mostly upgradient. The presence of this apparently diapycnal region is, at first sight, surprising since the diabatic terms are everywhere small in the interior. The reason there is a cross-isopycnal flux is as follows: the cross-isopycnal component of the eddy buoyancy flux can be related to a diabatic term and the advection of buoyancy variance:

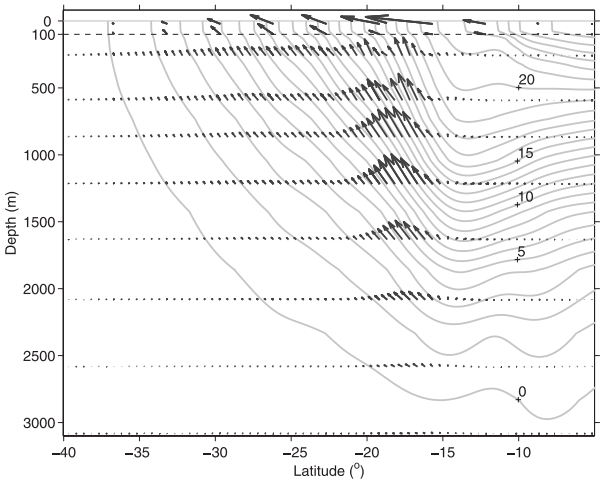

FIG. 5. Mean isotherms (which coincide with mean isopycnals) plotted as solid lines (contour interval 1°C) and eddy temperature flux $\overline{\mathbf{u}'T'}$ (arrows). In the surface diabatic layer (100 m thick) every other computational point in depth and every twenty-first latitude point is plotted; in the near-adiabatic interior every third latitude point is plotted. The longest arrow corresponds to a temperature flux of 0.077 m °C s^{-1}. The light solid line is the surface; the dashed line is the base of the surface diabatic layer.

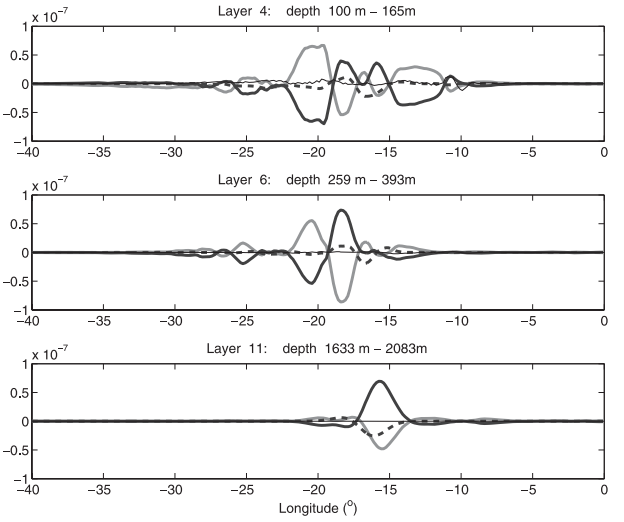

FIG. 6. Zonally and time-averaged eddy temperature variance budget for the three model layers at the top, middle, and close to the bottom of the near-adiabatic interior: diapycnal eddy temperature flux $\overline{\mathbf{u}'T'}\cdot\nabla\bar{T}$ (thick light line); advection of temperature variance by eddy velocity $-\nabla\cdot(\frac{1}{2}\overline{\mathbf{u}'T'^2})$ (thick dark line); advection of temperature variance by the mean velocity $-\bar{\mathbf{u}}\cdot\nabla(\frac{1}{2}\overline{T'^2})$ (thick dashed line). Note the importance of the triple correlation term $-\nabla\cdot(\frac{1}{2}\overline{\mathbf{u}'T'^2})$.

$$\overline{\mathbf{u}'b'}\cdot\nabla\bar{b}=\overline{b'Q'}-\left(\frac{\partial}{\partial t}+\bar{\mathbf{u}}\cdot\nabla\right)\left(\frac{1}{2}\overline{b'^2}\right)-\nabla\cdot\left(\frac{1}{2}\overline{\mathbf{u}'b'^2}\right), \tag{2}$$

where Q' is the diabatic source (or sink) of buoyancy. If the mean and eddy advection of the eddy buoyancy variance are negligible, there is, in a statistically steady state, a direct relationship between diapycnal eddy fluxes and local diabatic processes. However, analysis of the buoyancy variance budget shows that, in the region equatorward of the main jet, eddy advection (i.e., the triple correlation term) dominates the rhs of (2), as shown in Fig. 6.[1] Thus the cross-isopycnal fluxes in this instance are not, in fact, indicative of local diabatic processes but of the perturbation advection of buoyancy variance. Eddy buoyancy variance is largest in the region occupied by the strong eastward jet (Fig. 7). Local diabatic processes in this region are in fact almost negligible. Wilson and Williams (2004) and Olbers et al. (2000) pointed to the potential importance of the triple correlation terms in the PV budget.

d. Distribution of mean PV and thickness

Figure 8 shows the zonal and time-averaged thickness superposed on mean density (temperature) surfaces. Figure 9 shows the distribution of the zonally and time-averaged Ertel potential vorticity $\bar{P}=\overline{\zeta_a\cdot\nabla T}$, where ζ_a is the absolute vorticity, together with mean isopycnals (isotherms). Comparison of these figures shows that, in the region of active eddies, which is near and everywhere poleward of the main jet, it is PV rather than thickness that is homogenized along isopycnals.

It is clear in Fig. 9 that, in and poleward of the main jet, PV is homogenized[2] along the mean isopycnals in the near-adiabatic interior, but not near the surface. However, equatorward of about 12°S, where eddies are weak, strong along-isopycnal gradients of mean PV persist at the edge of the homogenized region. Close to the equator, where eddy activity is very small, thickness isolines are aligned with mean isotherms. Within the region of along-isopycnal PV homogenization, the mean PV field varies nonmonotonically with buoyancy. A tongue of strongly cyclonic PV extends downward and equatorward from the surface at about 23°S to a depth of about 1500 m at 15°S. Above the equatorward termination of this tongue lies the low PV pool noted above.

[1] Details in I. Cerovečki and J. M. Campine (2008, unpublished manuscript).

[2] We note that the PV shown in Fig. 9 is the unweighted mean PV, i.e., $\bar{P}=\overline{\zeta_a\cdot\nabla T}$ rather than the thickness-weighted mean $\bar{P}^*=\overline{\zeta}_a\cdot\nabla\overline{T}$. The latter is not as well homogenized within the jet as is the quantity shown in the figure.

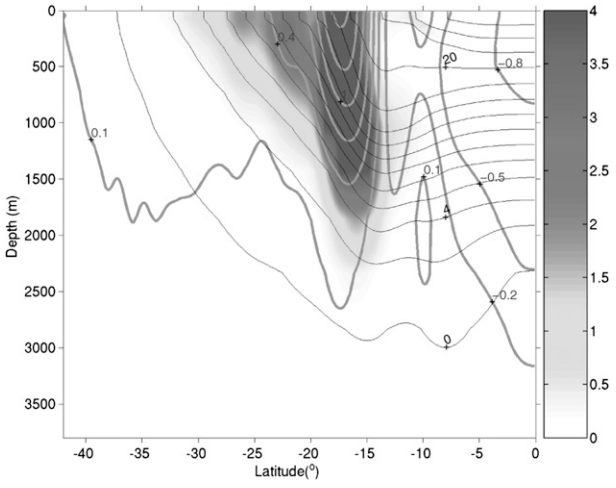

FIG. 7. Zonal- and time-mean eddy temperature variance [color, (°C)^2]. Also plotted are the mean isotherms (which coincide with the mean isopycnals) plotted as black thin lines (contour interval 2°C), and the mean zonal velocity contours (thick gray lines, m s^{-1}).

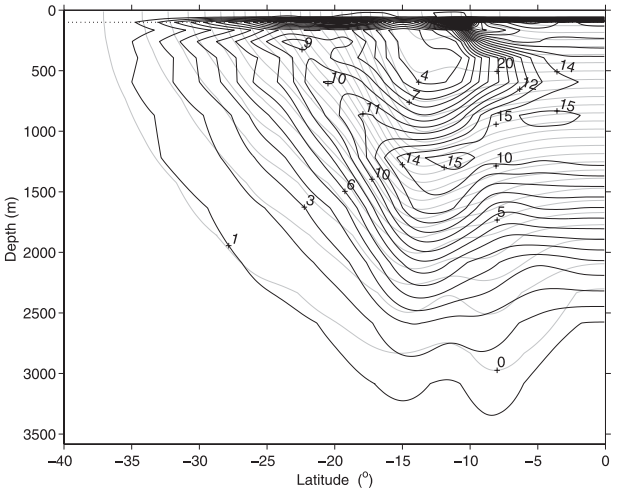

FIG. 8. Meridional cross section of $\partial\bar{T}/\partial z$ (the inverse of mean thickness with the contour interval 10^{-3} °C m^{-1}, dark solid line) and mean isotherms (which coincide with mean isopycnals) plotted as black thin lines (contour interval 1°C, light solid line). Dashed line is the mixed layer base.

4. Transformed Eulerian-mean analysis

a. Residual circulation

The TEM equations rely on the transformation from the Eulerian zonal mean velocity $\bar{\mathbf{u}}$ to the residual mean velocity $\bar{\mathbf{u}}^{\dagger}$, where

$$\bar{\mathbf{u}}^{\dagger} = \bar{\mathbf{u}} + \nabla \times \mathbf{i}\psi, \tag{3}$$

where $\mathbf{i}$ is the unit vector in the x direction and ψ is the "quasi-Stokes" streamfunction. Consider a quantity c that satisfies a mean conservation equation,

$$\bar{c}_t + \bar{\mathbf{u}} \cdot \nabla \bar{c} = -\nabla \cdot \mathbf{F}\{c\} + \overline{S\{c\}},$$

where $\mathbf{F}\{c\} = \overline{\mathbf{u}'c'}$ is the eddy flux of c and $\overline{S\{c\}}$ represent mean sources and sinks. Under the transformation (3), this equation becomes

$$\bar{c}_t + \bar{\mathbf{u}}^{\dagger} \cdot \nabla \bar{c} = -\nabla \cdot \mathbf{F}^{\dagger}\{c\} + \overline{S\{c\}},$$

where $\mathbf{F}^{\dagger}\{c\}$ is the "residual eddy flux" defined by

$$\mathbf{F}^{\dagger}\{c\} = \mathbf{F}\{c\} - \psi \mathbf{i} \times \nabla \bar{c}.$$

The first term is the "raw" eddy flux and, by introducing the second term, the eddy flux component parallel to c has been removed, leaving just the flux component along $\nabla \bar{c}$ in $\mathbf{F}^{\dagger}\{c\}$. An expression of this form was presented for trace chemicals by Andrews et al. (1987); Plumb and Ferrari (2005) provide more details.

Andrews and McIntyre (1978) introduced the coordinate-independent form of the quasi-Stokes streamfunction

$$\psi = -\frac{\mathbf{s} \cdot \overline{\mathbf{u}'b'}}{|\nabla \bar{b}'|} = \frac{-\overline{v'b'}\bar{b}_z + \overline{\omega'b'}\bar{b}_y}{\bar{b}_y^2 + \bar{b}_z^2}, \tag{4}$$

in which $\mathbf{s}$ is a unit vector parallel to the zonal mean isopycnal surface given by $\mathbf{s} = \mathbf{n} \times \mathbf{i}$ (where $\mathbf{n}$ is a unit vector normal to the zonal mean isopycnal surface so that $\mathbf{s}$ is northward, along the mean isopycnals, for stable stratification). Plumb and Ferrari (2005) argued that it is advantageous to use the definition (4) of the quasi-Stokes streamfunction in which the buoyancy flux and gradient are referenced to the local mean isopycnal slope, thus providing, in general, the cleanest separation of the cross-isopycnal and isopycnal flux components. They further showed, when using this definition of the quasi-Stokes streamfunction, that the surface boundary condition can be dealt with more readily than when using the quasigeostrophic (QG) definition of the quasi-Stokes streamfunction, because in the presence of a mixed layer where $\partial b/\partial z = 0$, isopycnals become locally vertical and (4) automatically satisfies a condition $\psi = 0$ at the upper boundary [in fact becoming the expression of Held and Schneider (1999) within the mixed layer]. However, Plumb and Ferrari (2005) noted that, while this condition (which really requires $|\partial b/\partial z| \ll |\partial b/\partial y|$) may be satisfied in laboratory systems like that analyzed by Kuo et al. (2005), it is unlikely to be met in systems with realistic aspect ratio (such as the case of interest here), where $|\partial b/\partial z| \gg \partial b/\partial y|$ even in the mixed layer.

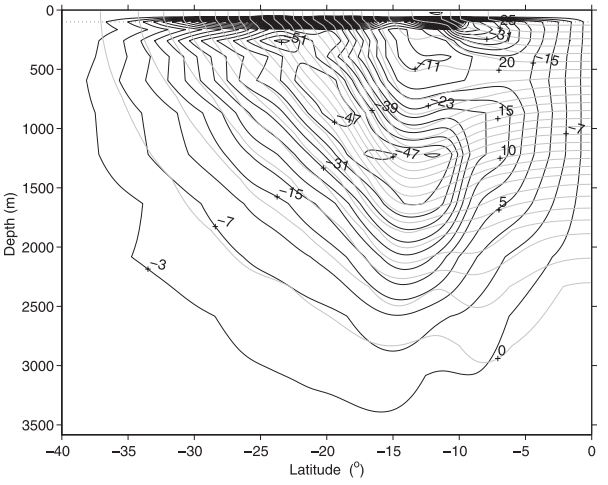

FIG. 9. Mean Ertel PV obtained as $\bar{P} = \overline{\zeta_a \cdot \nabla T}$ (dark solid line, contour interval 1.5×10^{-8} s^{-1} m^{-1} °C) and mean isopycnals (which coincide with the mean isotherms; plotted as light solid line, contour interval 1°C). Dashed line is the base of the mixed layer at 100-m depth.

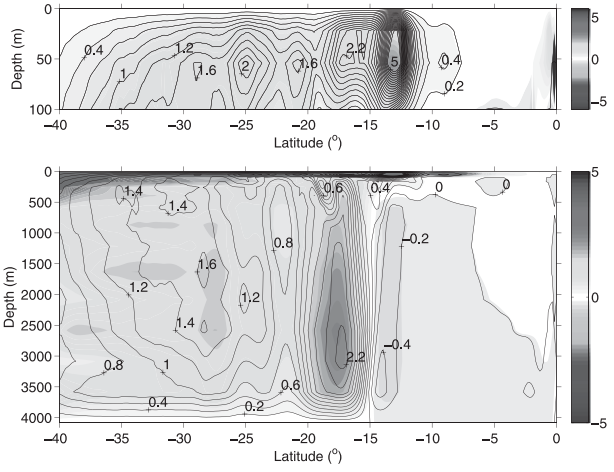

FIG. 10. Quasi-Stokes streamfunction (solid contour lines) defined by (5) compared to (top) the Held and Schneider (1999) streamfunction (solid contours) and (bottom) the QG streamfunction (solid contours); $\gamma = 10^3$ in (5). All in m^2 s^{-1}.

One way around this difficulty is to stretch coordinates in the vertical by a factor γ, the inverse of a representative aspect ratio, to make the aspect ratio of order unity in the stretched coordinates, in which case (4) becomes

$$\psi = \frac{-\overline{v'b'}\bar{b}_z + \gamma^2 \overline{w'b'}\bar{b}_y}{\gamma^2 \bar{b}_y^{\,2} + \bar{b}_z^{\,2}}. \tag{5}$$

Alternatively, we can exploit the inherent nonuniqueness in ψ. Plumb and Ferrari (2005) introduced a more general definition of the quasi-Stokes streamfunction:

$$\psi \equiv -\left|\nabla \bar{b}\right|^{-1}[\mathbf{s} \cdot \overline{\mathbf{u}'b'} - \alpha(\mathbf{n} \cdot \overline{\mathbf{u}'b'})]. \tag{6}$$

In fact, it is straightforward to show that (5) and (6) are equivalent if

$$\alpha = \frac{\epsilon(1-\gamma^2)}{1+\epsilon^2\gamma^2}, \tag{7}$$

where $\epsilon = -\bar{b}_y/\bar{b}_z$ is the mean isopycnal slope. Accordingly, we simply set γ equal to the aspect ratio $\gamma = 10^3$, which makes the interior isopycnal slopes of order unity in the stretched coordinate and makes the upper boundary condition on ψ very close to zero.

The advantage of working with the streamfunction as defined by (5) is that it is well defined in the regions where $\partial b/\partial z$ is very small and $\partial b/\partial y$ (being typically smaller than $\partial b/\partial z$ by the aspect ratio factor) is small as well. The disadvantage of working with the streamfunction (5) is that, by introducing nonzero value of α, the cleanest separation of the cross-isopycnal and isopycnal flux components characteristic of the streamfunction (4) is lost. Figure 10 shows that the quasi-Stokes streamfunction as defined by (5) does, indeed, produce a closed circulation. This streamfunction also agrees well with that of Held and Schneider (1999) close to the surface and with the conventional (quasigeostrophic) definition in the near-adiabatic interior, except that our form remains well defined and smooth both in the far south part of the basin as well as in the surface mixed layer where the stratification is very weak, whereas the latter takes on unrealistically large values. As shown in Fig. 11, the residual circulation thus defined is smooth, merges smoothly with the boundary conditions, and has about 10% of the Eulerian-mean transport in the interior. To a first approximation, the residual circulation is confined to the mixed layer.

The rigid meridional wall at the equator in the present calculation blocks the mean isopycnals (which coincide with the mean streamlines in the model ocean interior), preventing the development of appreciable residual circulation in the adiabatic interior. Since, of course, there is no equivalent of such a wall in the real ocean, this technical simplification, among many others (such as neglecting the continents), prevents us from directly relating our solutions to the real oceanic flow.

One way to avoid the equatorial wall would be to implement an open boundary condition. However, allowing the present flow to communicate with an adjacent basin by imposing an open boundary condition could introduce ambiguities in the flow solution since the boundary condition would depend on the assumptions made about the circulation in the other hemisphere.

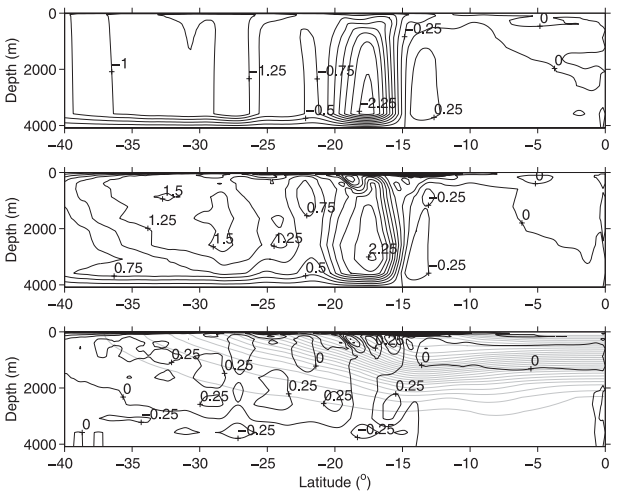

FIG. 11. Meridional cross section of zonally and time-averaged velocity streamfunctions: (top) Eulerian, (middle) quasi-Stokes streamfunction defined by (5), and (bottom) residual streamfunction. All in $m^2\ s^{-1}$. Contour interval is $0.25\ m^2\ s^{-1}$. Velocities are obtained as $v = \partial\psi/\partial z$, $w = -\partial\psi/\partial y$.

If such a calculation were to be extended to both hemispheres with wind and buoyancy forcing both symmetric around the equator and if both dissipation and bottom drag are sufficiently weak, potential vorticity conservation prevents fluid from crossing the equator and the flow would be the same as the flow analyzed here (for which slip is allowed at the equatorial wall). On the other hand, if latitudinally localized diabatic mixing, giving rise to diapycnal transport, were imposed, a nonzero residual circulation would develop on the side of the equator in which the mixing occurs. Even in the present model setup with an equatorial wall, such localized mixing gives rise to an asymmetric regime with significant residual circulation (I. Cerovečki and R. A. Plumb 2009, unpublished manuscript). However, unless the region of localized diabatic mixing includes the equator, the potential vorticity conservation will still prevent significant cross-equatorial residual flow in the zonally periodic geometry, confining the residual circulation to one hemisphere.[3]

Radko (2007) analyzed a zonally averaged oceanic flow (''aquaplanet'' model) extending over both hemispheres using the residual mean framework. The model atmosphere was interactive, so air–sea heat flux and wind stress responded to the changes in the sea surface temperature. The surface boundary conditions were symmetric about the equator, so one of the steady solutions is a symmetric flow characterized by absence of the interhemispheric buoyancy fluxes. However, such a flow was shown to be unstable, and the flow transitioned into asymmetric regime with significant interior flux of properties across the equator driven entirely by eddies.

Cross-equatorial meridional overturning residual circulation is, indeed, nonzero in more realistic models in which the basic flow is not zonally periodic (e.g., Ferreira and Marshall 2006).

On account of the geometry of the flow analyzed here, it may bear some resemblance to the Southern Ocean circulation. In this model ocean the residual circulation was essentially zero; previous papers (as Marshall and Radko 2003; Karsten and Marshall 2002; Marshall and Radko 2006) suggest that the residual circulation in the interior of the Southern Ocean is weak but not negligible. However, omission of any diabatic processes in the interior of the ocean as well as on the lateral boundaries, using highly idealized smooth forcing and modeling only one hemisphere, are simplifications that all result in inhibiting the residual circulation and prevent direct application of our results to the real ocean flow. The results of the present study should therefore be viewed as a stepping-stone to understanding the role of eddies in more complex and realistic flows rather being results directly applicable to ocean circulation.

b. Angular momentum flux

Figure 12 shows the residual eddy angular momentum flux $\mathbf{F}^{\dagger}\{m\}$, where $m = \Omega a^2 \cos^2\phi + ua\cos\phi$ is the specific angular momentum (in which u is the zonal component of velocity, a is the radius of the earth, and Ω is earth's angular rate of rotation), and

$$\mathbf{F}^{\dagger}\{m\} = \overline{\mathbf{u}'m'} - \psi\,\mathbf{i}\times\nabla\bar{m}. \tag{8}$$

The divergence of this flux represents the eddy forcing term in the TEM momentum equation

$$\frac{\partial\bar{m}}{\partial t} + \bar{\mathbf{u}}^{\dagger}\cdot\nabla\bar{m} = -\nabla\cdot\mathbf{F}^{\dagger}\{m\} + a\cos\phi\frac{\partial\tau_0}{\partial z}. \tag{9}$$

The surface wind stress input of zonal angular momentum τ_0 is shown in Fig. 1 with a maximum around 33°S. As, for example, in the *f*-plane case of Kuo et al. (2005), in the TEM budget it is vertical momentum transport by the eddies, not by the mean circulation, that transfers the wind stress downward to be removed by the bottom stress. In contrast to Kuo et al., however, there is also significant horizontal transport of zonal momentum by the eddies evident as the latitudinal component of $\mathbf{F}^{\dagger}\{m\}$, especially in the upper 500 m; zonal momentum is thus transferred predominantly into

[3] Unless numerical dissipation and/or bottom drag are sufficiently strong to invalidate PV conservation.

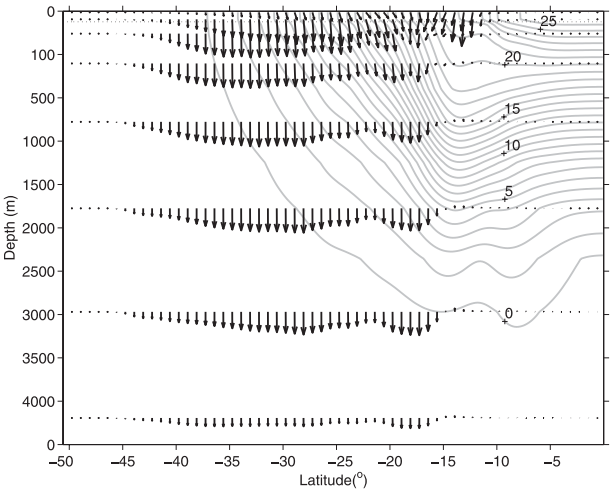

FIG. 12. Mean isotherms (plotted with contour interval 1°C) that coincide with the mean isopycnals (solid line) and residual angular momentum flux $\mathbf{F}^{\dagger}\{m\}$ (arrows): the longest arrow corresponds to a flux of size 1.84×10^4 m^3 s^{-2}; the dotted line is the base of the surface diabatic layer. Residual angular momentum flux is plotted for every other vertical layer starting from layer 1 and every fifth point in latitude.

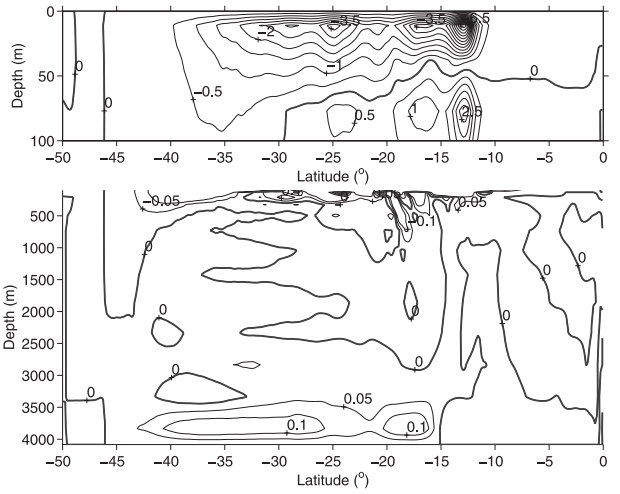

FIG. 13. Eddy forcing of mean angular momentum given by $-\nabla \cdot \mathbf{F}^{\dagger}\{m\}/(a\cos\phi)$ in (top) the surface diabatic layer and (bottom) the near-adiabatic interior in 10^{-6} m s^{-2}. Contour levels are (top) from -6.8 to 2.8 with contour interval of 0.5 m s^{-2} and (bottom) from -0.1 to 0.1 with contour interval of 0.05 m s^{-2}. Zero contour is plotted as a thick line.

the core of the main jet. Except close to the upper and lower boundaries, the flux is almost nondivergent, consistent with a very weak residual flow in the equilibrium state.

Plumb and Ferrari (2005) showed that, for small Rossby number but arbitrary isopycnal slope, there is a simple relationship between the TEM momentum flux divergence and the eddy PV and buoyancy fluxes. They used $\alpha = 0$ in the definition of ψ in (6); with our choice of nonzero α, the relationship becomes

$$\nabla \cdot \mathbf{F}^{\dagger}\{m\} = \frac{a\cos\phi}{|\nabla\bar{b}|}\left\{F^{\dagger(s)}\{p\} - \left[f\frac{\bar{b}_z^{\,2}}{|\nabla\bar{b}|^2}\left(\frac{\bar{b}_y}{\bar{b}_z}\right)_z - \frac{df}{dy}\frac{\bar{b}_y^{\,2}}{|\nabla\bar{b}|^2}\right]F^{\dagger(n)}\{b\}\right\} + f\frac{\partial}{\partial z}\left(\frac{\alpha}{|\nabla\bar{b}|}F^{\dagger(n)}\{b\}\right). \tag{10}$$

In Eq. (10) eddy forcing of the mean angular momentum has been expressed in terms of the fluxes of two materially conserved quantities—the cross-isopycnal flux of buoyancy and the isopycnal flux of PV.

Figure 13 shows eddy forcing of the mean angular momentum, given by $-\nabla \cdot \mathbf{F}^{\dagger}\{m\}$, diagnosed for our flow. The flux is almost nondivergent in the interior, except in the region of the main jet, above 1000-m depth and between about 13° and 20°S where, as already noted, the buoyancy fluxes have a significant cross-isopycnal component because of eddy advection of buoyancy variance. The flux is strongly divergent in the mixed layer and convergent near the bottom boundary, consistent with eddy angular momentum transfer by the form drag from the surface down to the bottom, as discussed above. In terms of the four terms on the rhs of (10), the second and third are negligible everywhere, consistent with scaling analysis which shows them to be significant only where the isopycnal slopes are of order unity (Plumb and Ferrari 2005). The first term, the isopycnal residual PV flux, provides the angular momentum flux convergence at the bottom, while both the first and last terms contribute to the net divergence in the near-jet interior region. The same two terms also contribute to the angular momentum flux divergence in the mixed layer; in fact, these terms largely cancel there, such that $\nabla \cdot \mathbf{F}^{\dagger}\{m\}$ is, in fact, a small residual of the two. Thus, for example, the Eliassen–Palm flux $-\mathbf{F}^{\dagger}\{m\}$ that is launched out of the surface layer is smaller than that implied by the near-surface heat fluxes alone. The importance of the near-boundary PV fluxes is consistent with the arguments of Schneider (2005), though here, at an upper boundary, the PV and heat flux contributions oppose each other, unlike the situation that prevails in Schneider's analysis of the lower boundary of an atmospheric model.

Finally, we note the consistency between the pattern of $\nabla \cdot \mathbf{F}^{\dagger}\{m\}$ of Fig. 13 and the residual circulation shown in Fig. 11, as is anticipated by the mean angular momentum budget (9). The near-zero residual flow in the interior, a consequence of weak diabatic effects there,

implies the vanishing of $\nabla \cdot \mathbf{F}^{\dagger}\{m\}$ there. Within the mixed layer there is a recirculating residual flow, driven equatorward by the surface wind stress and poleward below by the eddy flux divergence; the similar circulation near the bottom exists for the same reasons.

c. Eddy PV flux

Similar to the eddy heat flux, the eddy PV flux (not shown here) is skew almost everywhere in the near-adiabatic interior. Commenting on the same characteristic in their results, Kuo et al. (2005) pointed to the crucial distinction between the "raw" and "residual" eddy fluxes. In fact, (10) implies that the residual eddy PV flux vanish for adiabatic flow whenever mean PV is homogenized along the mean isopycnals, from which fact (8) makes it clear that the raw eddy flux, $\overline{\mathbf{u}'P'}$, in z coordinates must be skew.[4] In height coordinates, therefore, as noted by Plumb and Ferrari (2005) and Kuo et al. (2005), it is the residual flux that provides the basis for a downgradient flux parameterization. We shall return to this point in section 5d, but first we address the calculation of the appropriate measure of diffusivity. Determining the diffusivity from PV fluxes is problematic whenever the mean gradients are weak (e.g., Drijfhout and Hazeleger 2001) and so is not a useful approach here, nor does such a method give much insight into the processes producing the mixing. Accordingly, we shall take a different approach in section 5d.

5. Effective diffusivity as a diagnostic of mixing

a. Theoretical background

The term, effective diffusivity, was introduced by Nakamura (1996) and Winters and D'Asaro (1996), who showed that the combined effects of advection and diffusion, when described by the two-dimensional advection–diffusion equation for a passive tracer c along, for example, a nearly horizontal isopycnal surface in our model,

$$c_t + \mathbf{u} \cdot \nabla c = \nabla \cdot (\kappa \nabla c), \tag{11}$$

where $c(\mathbf{x}, t)$ is tracer concentration, κ is a constant diffusivity, and $\mathbf{u}(x, t)$ is a two-dimensional nondivergent velocity field, can be described exactly as a diffusion in tracer-based coordinates. Taking a "modified Lagrangian mean" approach, in which averages are taken along contours of the almost-conserved tracer, leads to the equation

$$\frac{\partial C}{\partial t} = \frac{1}{a^2 \cos\phi_e} \frac{\partial}{\partial \phi_e} \left[K_{\text{eff}} \cos\phi_e \frac{\partial C}{\partial \phi_e} \right], \tag{12}$$

where the "equivalent latitude" $\phi_e(C, t)$ of the contour of tracer concentration C is defined in terms of the area $A(C, t)$ enclosed by (poleward of) the contour such that $A = 2\pi a^2(1 - \sin\phi_e)$, where a is the earth's radius. (If the contour were an undisturbed latitude circle, ϕ_e would just equal the latitude of the contour.) The "effective diffusivity" K_{eff} is

$$K_{\text{eff}} = k \frac{L_e^2}{4\pi^2 a^2 \cos^2\phi_e} = k \frac{L_e^2}{L^2(\phi_e)}, \tag{13}$$

where $L(\phi_e) = 2\pi a \cos\phi_e$ is the length of the circle of latitude ϕ_e, and

$$L_e(C) = \sqrt{\oint |\nabla c| dl \oint \frac{dl}{|\nabla c|}} \tag{14}$$

is known as "equivalent length" of the contour (the integrals being around the contour).

From (14) one can see that effective diffusivity is a measure of the geometric complexity of a tracer field. Regions with weak mixing have small stretching rates, so the resulting geometric structure of the tracer field is simple, $L_e \sim L$, and the effective diffusivity is small. On the other hand, effective diffusivity is large if the geometric structure of the tracer field is complex, which is in turn the result of large stretching rates typical for regions with strong mixing. Haynes and Shuckburgh (2000a,b) and Allen and Nakamura (2001) have applied this method to diagnose transport and mixing properties in the stratosphere and troposphere. Marshall et al. (2006) used the same method to estimate surface diffusivities associated with geostrophic eddies in the Southern Ocean by numerically monitoring lengthening of idealized tracer contours that were being strained by surface geostrophic flow observed by satellite altimetry. Here, we use this method to diagnose mixing properties of the flow with the goal of understanding tracer dynamics for application to a parameterized model.

b. Application to idealized tracer field

The model was run with a tracer whose concentration in the uppermost model layer only was relaxed with relaxation time one month to a specified latitudinal profile, with concentration increasing linearly with latitude from zero at 50.67°S to one at the equator; a Laplacian horizontal tracer diffusivity $\kappa = 30\ \text{m}^2\ \text{s}^{-1}$ was

[4] Note that this is true of Ertel PV; the northward flux of quasigeostrophic PV vanishes in such circumstances.

included. Coefficients of effective diffusivity were diagnosed using (13) and (14) from the modeled tracer field. After an initial adjustment period we analyzed 40 snapshots of tracer concentration taken at regular time intervals of 1 yr starting 30 years after tracer release.

Since we expect the processes of stirring and mixing to occur within isopycnal surfaces under the near-adiabatic conditions that characterize the flow interior (i.e., away from the surface diabatic layer), we analyze tracer distributions on 67 isothermal (isopycnal) surfaces. A balance between advection and diffusion occurs on the scale $\sqrt{k/S}$, where S is the strain rate, which can be approximated by the ratio of V/L, where V and L are typical scales for eddy speed and size. The dominant eddy is as large as geometry permits, so L is approximately 10° longitude, and a typical velocity scale is 0.1–0.2 m s^{-1}, which gives a dissipative length scale of approximately 15 km, very close to the model grid scale.

c. *Effective diffusivity: Results and discussion*

Figure 14 shows instantaneous effective diffusivity estimates (top panel) obtained by analyzing a snapshot of tracer concentration on an instantaneous isopycnal surface (T = 1.3°C, bottom panel). The mixing regions are characterized by tracer concentration contours that are vigorously stretched into complex geometrical shapes with tight gradients: one highly stirred region is between 15° and 20°S where the tracer concentration contours are stretched to enclose large areas and another is poleward of 25°S latitude. Poleward of about 33°S, effective diffusivity estimates could not be obtained on this isothermal surface because the surface outcrops and the tracer contours are no longer closed. Equatorward of 12°S and in the region around 23°–24°S the smoothness of the tracer contours is reflected in small values of effective diffusivity.

Figure 15 shows effective diffusivity estimates obtained as the zonal and time average of a set of instantaneous effective diffusivity estimates diagnosed on instantaneous isopycnal surfaces. Contours of the zonal-mean zonal velocity are overlaid to illustrate the underlying flow structure. Light lines show the isopycnal surfaces on which effective diffusivity calculation has been carried out and the thick light line is the isothermal surface analyzed in the previous figure.

Figure 15 shows strong spatial inhomogeneity in the distribution of effective diffusivity, which in the upper 2000 m is large on the equatorward side of the strong eastward jet and, at greater depths, beneath the jet and on the poleward side of the jet. Centered on the core of the jet is a band of very low effective diffusivity. In the jet core region, the jet simply meanders in time, thus not giving rise to much mixing. Surface temperature contours, shown in Fig. 4, illustrate this behavior: in the region of the strong eastward jet (15°–20° latitude) temperature contours are very smooth, whereas on the equatorward side of the jet temperature contours are vigorously stretched, folded, and wrapped around the large eddy, giving rise to strong temperature gradients and strong mixing. Therefore, the region of high effective diffusivity does not coincide with the region of strongest eddy activity (e.g., heat flux, temperature variance), which was shown to coincide with the region occupied by the strong eastward jet (Figs. 5 and 7), but reflects where chaotic stirring is most vigorous, in the wings of the jet (cf. Fig. 4). Indeed, as shown in Fig. 15, the band of large K_{eff} coincides approximately with the 0.1 m s^{-1} velocity contour.

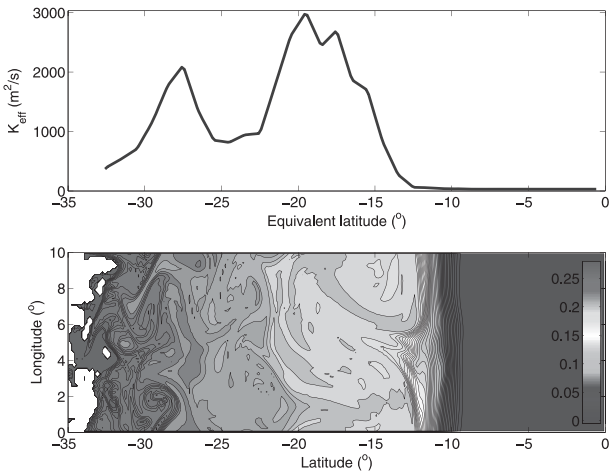

FIG. 14. (top) Instantaneous effective diffusivity (m^2 s^{-1}) obtained by analyzing (bottom) a snapshot of passive tracer concentrations on 1.3°C isotherm 70 yr after tracer release.

Weak mean field gradients do not necessarily imply strong mixing. In the core of the strong eastward jet PV gets homogenized even though the diffusivity is weak there since the residual mean velocity is negligible so that there are no processes to restore the mean PV gradient; even weak mixing was sufficient to wipe out the mean gradients.

This spatial pattern of effective diffusivity is consistent with the theory of Rossby wave critical layers (Haynes 1985), which shows that particle displacements are large near the critical line where the Doppler-shifted phase speed is small. This pattern of weak eddy diffusivities inside the jet and strong diffusivities outside the jet is also consistent with analysis of observed geophysical flows: Haynes and Shuckburgh (2000a) diagnosed transport and mixing properties of the isentropic flow in the lower and middle stratosphere using observed winds to advect tracer on isentropic surfaces. They showed that the stratospheric polar jet is characterized

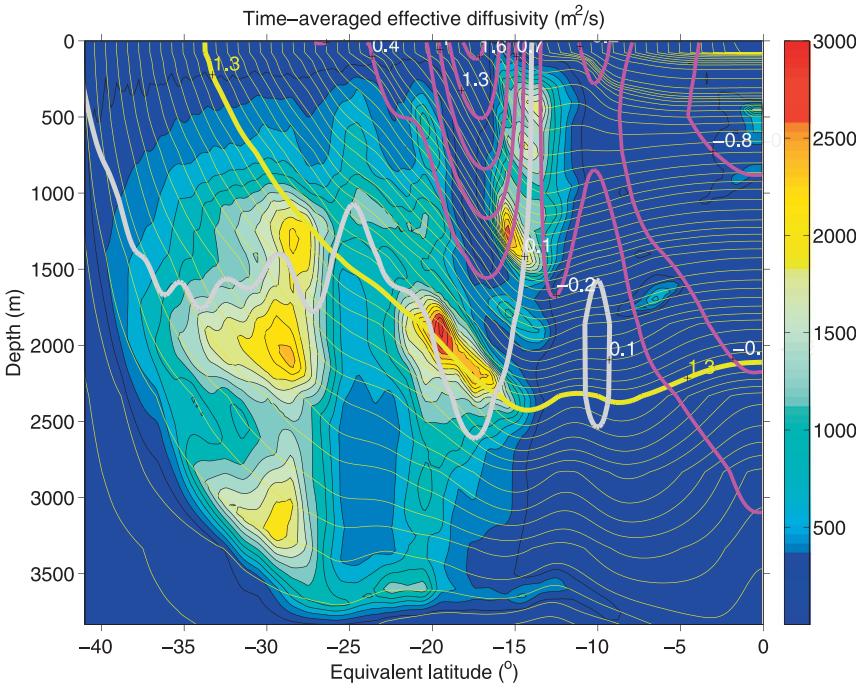

FIG. 15. Time and zonally averaged effective diffusivity ($m^2\ s^{-1}$) obtained by analyzing snapshots of passive tracer concentration taken 1 yr apart from 31 to 71 yr after tracer release (colors) together with time and zonally averaged zonal velocity (magenta line, $m\ s^{-1}$) and time and zonally averaged isotherms on which calculation has been carried out (yellow lines, °C). Thick yellow line is the 1.3°C isotherm; thick light gray line is the 0.1 $m\ s^{-1}$ zonal velocity isoline.

by low diffusivities, thus representing a strong barrier to mixing near the core of the jet and large diffusivities in the weaker mean flow equatorward of the jet. Similarly, Marshall et al. (2006) estimated near-surface eddy diffusivities associated with geostrophic eddies in the Southern Ocean by numerically monitoring the lengthening of idealized tracer contours, which were advected by surface geostrophic flow observed by satellite altimetry. They obtained large diffusivities (2000 $m^2\ s^{-1}$) on the equatorward flank of the Antarctic Circumpolar Current and small diffusivities (500 $m^2\ s^{-1}$) at the jet axis.

The contrast, evident in Fig. 15, between weak mixing at the core of the surface jet and strong mixing beneath the jet, is consistent with observations of the Gulf Stream. Bower et al. (1985) showed that in the upper thermocline the transition of water properties inside and outside the Gulf Stream jet region is sharp, suggesting that water mass exchanges across the Gulf Stream slope water front are limited at these levels. Below this region deep property fields are being efficiently homogenized by mesoscale exchanges across the Gulf Stream.

Note that the effective diffusivities are also generally large in the region poleward of −15° latitude, which is the region where the strong eddies have homogenized PV on the isopycnal surfaces (Fig. 9).

d. *PV transport and the apparent horizontal diffusivity for buoyancy*

The effective diffusivity expresses the rate of transport along isopycnal surfaces of almost-conserved tracers by the stirring of tracer variance. In the adiabatic interior, though not in the near-surface diabatic layer, this along-isopycnal process must dominate eddy transport: We therefore anticipate the horizontal component of the residual eddy flux of PV (Plumb and Ferrari 2005) in height coordinates to be

$$F_y^{\dagger}\{P\} = \overline{v'P'} + \psi\bar{P}_z = -K_{\text{eff}}\,\bar{P}_y|_{\bar{b}}. \qquad (15)$$

As discussed by Kuo et al. (2005), in the absence of any significant residual circulation to provide a mean flux of PV, equilibrium demands that the eddy flux be zero, whereas (15) requires that $\bar{P}_y|_{\bar{b}} = 0$, wherever K_{eff} is finite, as we found (Fig. 9). One unfortunate consequence of this is that, like Drijfhout and Hazeleger (2001), we cannot verify this relationship directly from the model: both sides of (15) being essentially zero in the interior.

We can, however, investigate the implications of (15) for the eddy buoyancy fluxes (limited though we shall find these implications to be). In principle, since the raw eddy buoyancy fluxes in the interior are skew (Fig. 5), it is unsound in principle to parameterize them as downgradient. Nevertheless, just as in the quasigeostrophic case (e.g., Treguier et al. 1997), one can, under certain approximations, obtain a relationship between the northward eddy flux of buoyancy and its mean northward gradient, starting with the flux–gradient relationship for PV. The derivation carries over (under the same assumptions) to the case of finite isopycnal slope. Assuming planetary geostrophic scaling so that $P = fb_z$ and assuming $|\bar{b}_y| \ll |\bar{b}_z|$ so that $\psi = -\overline{v'b'}/\bar{b}_z$, we have

$$\overline{v'P'} + \psi\bar{P}_z = f(\overline{v'b'})_z - \frac{\overline{v'b'}}{\bar{b}_z} f\bar{b}_{zz} = f\bar{b}_z\left(\frac{\overline{v'b'}}{\bar{b}_z}\right)_z,$$

where we have invoked the thermal wind balance to infer that $\overline{v'b'}_z = (\overline{v'b'})_z$, while

$$\bar{P}_y|_{\bar{b}} = \bar{P}_y - \frac{\bar{b}_y}{\bar{b}_z}\bar{P}_z = f\bar{b}_z\left(\frac{\beta}{f} + \epsilon_z\right),$$

where $\epsilon = -\bar{b}_y/\bar{b}_z$ is the mean isopycnal slope. Then (15) gives

$$\left(\frac{\overline{v'b'}}{\bar{b}_z}\right)_z = -K_{\text{eff}}\left(\frac{\beta}{f} + \epsilon_z\right). \tag{16}$$

The final step, to obtain the buoyancy flux–gradient relationship

$$\overline{v'b'} = -K_{\text{eff}}\bar{b}_y, \tag{17}$$

requires the more severe assumptions of neglecting (i) β compared with $f\epsilon_z$ in (16), (ii) vertical variations of K_{eff}, and (iii) the integration constant consequent on integrating (16) with respect to z. Each of these assumptions is difficult to justify. In fact, in our example with $\bar{P}_y|_{\bar{b}} = 0$ throughout much of the interior, the rhs of (16) actually vanishes and the neglected integration constant is paramount. Note also that, since (15) is not valid in the diabatic near-surface layer, neither is (17).

The result of determining a diffusivity for buoyancy from the model output by inverting a flux-gradient relationship like (17) is shown in Fig. 16. The inversion is, of course, problematic where the mean gradient vanishes, as is evident in the figure. Overall, while the magnitudes of the apparent diffusivity of buoyancy are similar to those of K_{eff}, the structures are rather different: the absence of a region of strong apparent diffusivity on the equatorward flank of the main jet and of a minimum in the core are the most striking discrepancies. The large values near the surface reflect diabatic fluxes, which will be addressed in section 5e.

This comparison exemplifies the limitations of using a flux-gradient relationship for buoyancy. Following Treguier et al. (1997), we note that a sufficient specification of the role of the eddies on the mean state is one of PV mixing in the interior plus a representation of diabatic buoyancy transport near the surface. [In fact, if PV is homogenized in the interior, the mean state is then determined by this fact and the near-surface buoyancy fluxes, as described by Kuo et al. (2005).]

e. Diapycnal eddy diffusivity

While the effective diffusivity expresses the rates of stirring and mixing along isopycnal surfaces, it yields no information on diapycnal transport consequent on diabatic processes. We could, in principle, calculate a diapycnal diffusivity from an assumed diapycnal flux-gradient relationship for buoyancy but, since the eddy buoyancy fluxes are so close to being skew throughout most of the domain, quantification of the diapycnal component is prone to error. Accordingly, in order to preserve the relationship between diapycnal transport and diabatic processes, we follow the approach of Medvedev and Greatbatch (2004), expressing the diapycnal diffusivity as $\kappa = -(\nabla\bar{b})^{-2}\overline{Q'b'}$, where Q' is the eddy component of the local diabatic buoyancy source or sink; $\overline{Q'b'}$ is obtained from $\overline{Qb} - \bar{Q}\bar{b}$. The resulting estimate for κ is shown in Fig. 17. As expected, the eddy-induced diapycnal diffusivity in our flow is strongest in the surface diabatic layer where the diabatic forcing is applied. More surprisingly, it is also significant in the region immediately below the surface south of 15°S where ocean is on average losing heat to the atmosphere, resulting in frequent convection in the upper part of the water column. As mentioned in section 5a, this colder water then sinks all the way to the bottom of the ocean in the southernmost part of the basin, filling up the bottom of the basin with the densest water in the flow and giving rise to elevated values of diapycnal eddy diffusivity. (South of 35°S in the uppermost layer the eddy-induced diffusivity becomes as large as 1000 $m^2\ s^{-1}$, which is the value of vertical diffusivity associated with convective episodes used in the model.) Frequent convective episodes in the surface layers in the latitude range 13°–17°S feed the low PV pool formed in the temperature range 20°–21°C (section 3b), resulting in an average eddy diffusivity of 3 $m^2\ s^{-1}$ in the uppermost layers.

6. Conclusions

Although the modeled flow described here is not a very realistic representation of oceanic flow, it develops

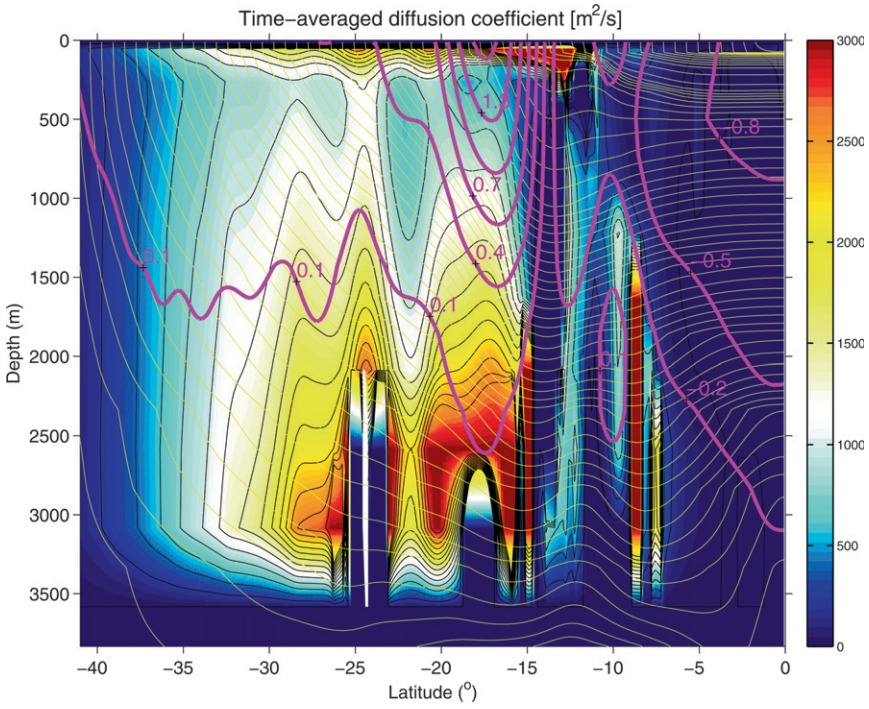

FIG. 16. Point estimates of the apparent horizontal diffusivity for buoyancy ($m^2\ s^{-1}$) obtained from flux–gradient relationship $-\overline{v'T'}/\bar{T}_y$, where $\overline{v'T'}$ is the meridional eddy temperature flux and $\bar{T}_y$ is the mean meridional temperature gradient; time- and zonally averaged zonal velocity (magenta line, contour interval 0.3 m s^{-1}) and time- and zonally averaged isotherms (yellow lines, °C).

a number of dynamical features that may be relevant in understanding some of the characteristics of eddy transport in the ocean. The model flow stratification and flow speeds are realistic. The flow develops a number of persistent zonal jets in statistically steady state, with the eddies playing an important role in redistributing angular momentum both horizontally and, especially, vertically. A further prominent feature of the flow is a strong and persistent eddy that has a Kelvin cat's eye structure. The eddy is very large in size, typically occupying the zonal width of the basin, situated on the equatorward side of the main eastward jet at latitudes 15° to 10°S. Smaller eddies develop farther poleward.

Running the experiment in spherical geometry over a large latitude band showed clearly that eddy processes homogenize PV and not thickness along the mean buoyancy contours in the near-adiabatic interior everywhere in the basin where eddies have developed—that is, near and poleward of the most energetic eastward jet.

In the vicinity of the main jet, triple correlation terms in the buoyancy variance budget are large, giving rise to a significant cross-isopycnal component of eddy buoyancy flux. The mean advection of buoyancy variance is not a dominant term in this balance. This situation is in contrast to the frequent neglect of triple correlation terms in the literature. Redefining the streamfunction to include not only the mean advection of buoyancy variance parallel to the isopycnals (as suggested by Marshall and Shutts 1981; McDougall and McIntosh 1996, 2001) but also triple correlation terms (as suggested by Greatbatch 2001) did not uniformly reduce the cross-isopycnal component of eddy buoyancy flux in this flow.

We have diagnosed eddy mixing and transport properties of the flow by applying the effective diffusivity diagnostics introduced by Nakamura (1996) and Winters and D'Asaro (1996). The along-isopycnal effective diffusivities are spatially very inhomogeneous: they are large on the equatorward side of the strong eastward jet, beneath the jet, and on the poleward side of the jet. In the core of the jet eddy mixing rates are very low. Thus, the region of high effective diffusivity does not coincide with the region of the strongest eddy activity centered on the strong eastward jet.

In the jet, eddy behavior is predominantly wavelike, so, although the eddy fluxes are very large there, there is little stirring. In the wings of the jet, however, stirring is vigorous, characterized by large particle displacements. This spatial pattern of effective diffusivity is consistent with critical layer theory and with analysis of atmospheric and oceanic flows. Omission of any diabatic

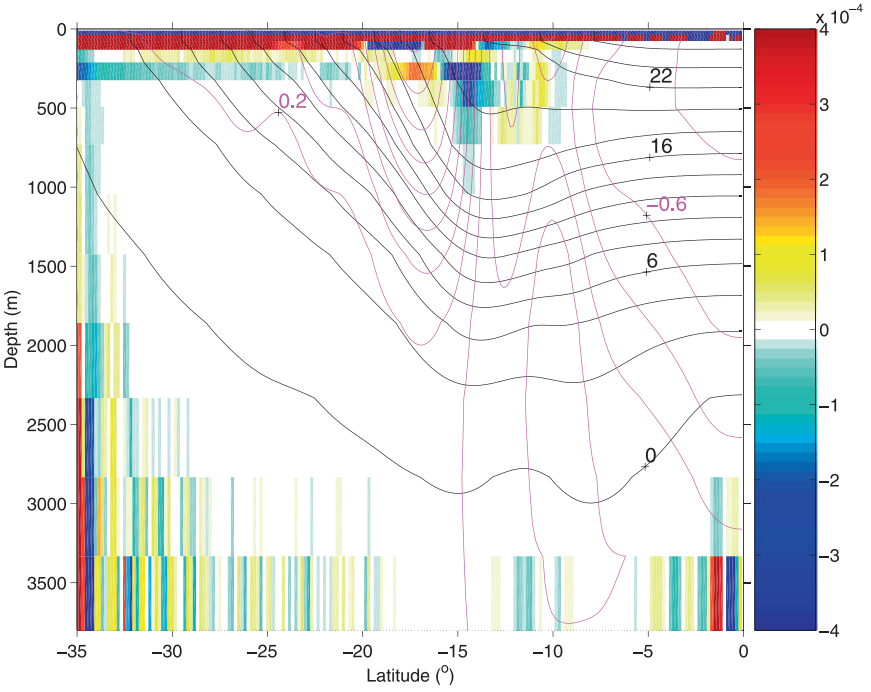

FIG. 17. Point estimates of diapycnal eddy-induced diffusivity ($m^2\ s^{-1}$) obtained following Medvedev and Greatbatch (2004) as in section 5e; time- and zonally averaged isotherms (black lines, °C) and time- and zonally averaged zonal velocity (magenta line, contour interval 0.2 $m\ s^{-1}$).

processes in the interior of the ocean as well as on the lateral boundaries, the imposition of highly idealized smooth forcing, and the modeling of only one hemisphere are all simplifications introduced in this analysis, which prevent direct application of our results to the real ocean flow. Particularly the rigid meridional wall at the equator in the present calculation, blocking the mean isopycnals (which coincide with the mean streamlines in the model ocean interior), prevents appreciable residual circulation from developing in the adiabatic interior. Since, of course, there is no equivalent of such a wall in the real ocean, this technical simplification, among many others (such as neglecting the continents), prevents us from directly relating our solutions to the real oceanic flow.

On account of the geometry of the flow, our flow may bear some resemblance to that of the Southern Ocean, but, as noted above, in our model ocean the residual circulation was essentially zero, whereas the residual circulation in the interior of the Southern Ocean is weak, but not negligible (e.g., Marshall and Radko 2003; Karsten and Marshall 2002; Marshall and Radko 2006). Thus the results of the present study should be viewed as a stepping-stone to understanding of the role of eddies in more complex and realistic flows rather than as results directly applicable to ocean circulation.

Acknowledgments. IC would like to thank Jean-Michel Campine, whose generous help with numerous numerical issues was most precious, as well as Timour Radko and an anonymous reviewer, whose suggestions considerably improved the paper. We acknowledge support from NSF, under Grant OCE-0426307.

REFERENCES

Allen, D. R., and N. Nakamura, 2001: A seasonal climatology of effective diffusivity in the stratosphere. *J. Geophys. Res.,* **106,** 7917–7935.

Andrews, D. G., and M. E. McIntyre, 1978: Generalized Eliassen-Palm and Charney-Drazin theorems for waves on axisymmetric mean flows in compressible atmospheres. *J. Atmos. Sci.,* **35,** 175–185.

——, J. R. Holton, and C. B. Leovy, 1987: *Middle Atmosphere Dynamics*. Academic Press, 489 pp.

Bower, A. S., H. T. Rossby, and J. L. Lillibridge, 1985: The Gulf Stream—Barrier or blender? *J. Phys. Oceanogr.,* **15,** 24–32.

Cerovečki, I., and J. Marshall, 2008: Eddy modulation of air–sea interaction and convection. *J. Phys. Oceanogr.,* **38,** 65–83.

Chan, C. J., R. A. Plumb, and I. Cerovečki, 2007: Annular modes in a multiple migrating zonal jet regime. *J. Atmos. Sci.,* **64,** 4053–4068.

Drijfhout, S. S., and W. Hazeleger, 2001: Eddy mixing of potential vorticity versus thickness in an isopycnic ocean model. *J. Phys. Oceanogr.,* **31,** 481–505.

Eden, C., R. J. Greatbatch, and D. Olbers, 2007a: Interpreting eddy fluxes. *J. Phys. Oceanogr.,* **37,** 1282–1296.

——, ——, and J. Willebrand, 2007b: A diagnosis of thickness fluxes in an eddy-resolving model. *J. Phys. Oceanogr.,* **37,** 727–742.

Ferreira, D., and J. Marshall, 2006: Formulation and implementation of a ''residual-mean'' ocean circulation model. *Ocean Modell.,* **13,** 86–107.

Gent, P. R., and J. C. McWilliams, 1990: Isopycnal mixing in ocean circulation models. *J. Phys. Oceanogr.,* **20,** 150–155.

——, J. Willebrand, T. J. McDougall, and J. C. McWilliams, 1995: Parameterizing eddy-induced tracer transports in ocean circulation models. *J. Phys. Oceanogr.,* **25,** 463–474.

Greatbatch, R. J., 1998: Exploring the relationship between eddy-induced transport velocity, vertical momentum transfer, and the isopycnal flux of potential vorticity. *J. Phys. Oceanogr.,* **28,** 422–432.

——, 2001: A framework for mesoscale eddy parameterization based on density-weighted averaging at fixed height. *J. Phys. Oceanogr.,* **31,** 2797–2806.

Haynes, P. H., 1985: Nonlinear instability of a Rossby-wave critical layer. *J. Fluid Mech.,* **161,** 493–511.

——, and E. Shuckburgh, 2000a: Effective diffusivity as a diagnostic of atmospheric transport 1. Stratosphere. *J. Geophys. Res.,* **105,** 22 777–22 794.

——, and ——, 2000b: Effective diffusivity as a diagnostic of atmospheric transport 2. Troposphere and lower stratosphere. *J. Geophys. Res.,* **105,** 22 795–22 810.

Held, I. M., and T. Schneider, 1999: The surface branch of the zonally averaged mass transport circulation in the troposphere. *J. Atmos. Sci.,* **56,** 1688–1697.

Karsten, R. H., and J. Marshall, 2002: Constructing the residual circulation of the ACC from observations. *J. Phys. Oceanogr.,* **32,** 3315–3327.

——, H. Jones, and J. Marshall, 2002: The role of eddy transfer in setting the stratification and transport of a circumpolar current. *J. Phys. Oceanogr.,* **32,** 39–54.

Kuo, A., R. A. Plumb, and J. Marshall, 2005: Transformed Eulerian-mean theory. Part II: Potential vorticity homogenization and the equilibrium of a wind- and buoyancy-driven zonal flow. *J. Phys. Oceanogr.,* **35,** 175–187.

Kushner, P. J., and L. M. Polvani, 2004: Stratosphere–troposphere coupling in a relatively simple AGCM: The role of eddies. *J. Climate,* **17,** 629–639.

Marshall, J., and G. Shutts, 1981: A note on rotational and divergent eddy fluxes. *J. Phys. Oceanogr.,* **11,** 1677–1680.

——, and T. Radko, 2003: Residual-mean solutions for the Antarctic Circumpolar Current and its associated overturning circulation. *J. Phys. Oceanogr.,* **33,** 2341–2354.

——, and ——, 2006: A model of the upper branch of the meridional overturning of the southern ocean. *Prog. Oceanogr.,* **70,** 331–345.

——, A. Adcroft, C. Hill, L. Perelman, and C. Heisey, 1997a: A finite-volume, incompressible Navier Stokes model for studies of the ocean on parallel computers. *J. Geophys. Res.,* **102** (C3), 5753–5766.

——, C. Hill, L. Perelman, and A. Adcroft, 1997b: Hydrostatic, quasi-hydrostatic, and nonhydrostatic ocean modeling. *J. Geophys. Res.,* **102** (C3), 5733–5752.

——, E. Shuckburgh, H. Jones, and C. Hill, 2006: Estimates and implications of surface eddy diffusivity in the Southern Ocean derived from tracer transport. *J. Phys. Oceanogr.,* **36,** 1806–1821.

McDougall, T. J., and P. C. McIntosh, 1996: The temporal-residual-mean velocity. Part I: Derivation and the scalar conservation equations. *J. Phys. Oceanogr.,* **26,** 2653–2665.

——, and ——, 2001: The temporal-residual-mean velocity. Part II: Isopycnal interpretation and the tracer and momentum equations. *J. Phys. Oceanogr.,* **31,** 1222–1246.

Medvedev, A. S., and R. J. Greatbatch, 2004: On advection and diffusion in the mesosphere and lower thermosphere: The role of rotational fluxes. *J. Geophys. Res.,* **109,** D07104, doi: 10.1029/2003JD003931.

Nakamura, N., 1996: Two-dimensional mixing, edge formation, and permeability diagnosed in an area coordinate. *J. Atmos. Sci.,* **53,** 1524–1537.

Olbers, D., J.-O. Wolff, and C. Völker, 2000: Eddy fluxes and second-order moment balances for nonhomogeneous quasi-geostrophic turbulence in wind-driven zonal flows. *J. Phys. Oceanogr.,* **30,** 1645–1668.

Panetta, R. L., 1993: Zonal jets in wide baroclinically unstable regions: Persistence and scale selection. *J. Atmos. Sci.,* **50,** 2073–2106.

Plumb, R. A., and R. Ferrari, 2005: Transformed Eulerian-mean theory. Part I: Nonquasigeostrophic theory for eddies on a zonal-mean flow. *J. Phys. Oceanogr.,* **35,** 165–174.

Radko, T., 2007: A mechanism for establishment and maintenance of the meridional overturning in the upper ocean. *J. Mar. Res.,* **65,** 85–116.

——, and J. Marshall, 2004: Eddy-induced diapycnal fluxes and their role in the maintenance of the thermocline. *J. Phys. Oceanogr.,* **34,** 372–383.

Schneider, T., 2005: Zonal momentum balance, potential vorticity dynamics, and mass fluxes on near-surface isentropes. *J. Atmos. Sci.,* **62,** 1884–1900.

Thompson, D. W. J., and J. M. Wallace, 2000: Annular modes in the extratropical circulation. Part I: Month-to-month variability. *J. Climate,* **13,** 1000–1016.

Treguier, A. M., I. M. Held, and V. D. Larichev, 1997: On the parameterization of the quasigeostrophic eddies in primitive ocean models. *J. Phys. Oceanogr.,* **27,** 567–580.

Visbeck, M., J. Marshall, T. Haine, and M. Spall, 1997: Specification of eddy transfer coefficients in coarse-resolution ocean circulation models. *J. Phys. Oceanogr.,* **27,** 381–402.

Wilson, C., and R. G. Williams, 2004: Why are eddy fluxes of potential vorticity difficult to parameterize? *J. Phys. Oceanogr.,* **34,** 142–155.

Winters, K. B., and E. A. D'Asaro, 1996: Diascalar flux and the rate of fluid mixing. *J. Fluid Mech.,* **317,** 179–193.